PERGAMON

Chemical Engineering Science 58 (2003) 1531–1543

Chemical Engineering Science

www.elsevier.com/locate/ces

Modeling of sedimentation of polydisperse spherical beads with a broad size distribution

Bo Xue, Yan Sun*

Department of Biochemical Engineering, School of Chemical Engineering and Technology, Tianjin University, Tianjin 300072, China

Received 26 March 2002; received in revised form 22 July 2002; accepted 4 September 2002

Abstract

This article deals with experimental and theoretical studies of the sedimentation of polydisperse agarose beads with broad particle size distributions. A light-extinction principle was used to measure the variation of solid concentration in the suspension with time and settling distance. Different experimental conditions have been used to show the influence of solid concentration and liquid density and viscosity on the settling behavior of the beads. The sedimentation process was described mathematically by a system of conservation law using Masliyah's hindered settling function. The physical properties of the beads and the optical properties of the suspension were carefully examined to enable a reliable comparison between experimental and simulation results. The model gives good predictions under all the conditions studied, showing its soundness in formulating the hindered settling process of polydisperse particles in a suspension.

Keywords: Sedimentation; Suspension; Modeling; Particle; Particle size distribution; Simulation

1. Introduction

Sedimentation of solid particles in a fluid is a common phenomenon with numerous applications in chemical and civil engineering, geology, metallurgy and oceanography, and has been extensively studied for decades (Wallis, 1969; Khan & Richardson, 1989; Huppert, Kerr, Lister, & Turner, 1991). A few examples of its applications in chemical industry include fluidized bed reactors, settling tanks, and hydraulic conveying. With the development of expanded bed adsorption (EBA) technology (Anspach, Curbelo, Hartmann, Garke, & Deckwer, 1999), this phenomenon has aroused new interests among biochemical engineers. As a promising unit operation that integrates product capture, clarification, concentration and purification in a single step, EBA has become one of the best choices for recovering bioproducts, for example proteins and enzymes, from whole-cell fermentation broths or cell homogenates (Batt, Yabannavar, & Singh, 1995; Owen & Chase, 1997; Clemmitt & Chase, 2000). The hydrodynamics of an EBA system needs to be well characterized because it is of paramount importance to the quantity and quality of the desired products. Some pioneer work has been done to study experimentally axial variations in adsorbent size, bed voidage, and liquid dispersion within an EBA column (Willoughby, Hjorth, & Titchener-Hooker, 2000; Bruce & Chase, 2001), providing valuable information on solid–liquid suspensions. At the same time, it issues a formidable challenge, that is, to interpret the experimental results with the existing sedimentation theories, to not only chemical engineers but also hydrodynamicists and mathematicians.

Complications in modeling the settling of a solid–liquid suspension of practical importance arise to a great extent from the wide variety of sizes, shapes, and densities of the particles and particle–particle interactions (Wallis, 1969). To simplify experimental and theoretical analyses, to date most publications on suspension sedimentation have focused primarily on spherical monodisperse particles or particle mixtures consisting of two or three kinds of particles with far different sizes and/or densities (Law, Masliyah, MacTaggart, & Nandakumar, 1987; Davis & Birdsell, 1988; Cheung, Powell, & McCarthy, 1996; Galvin, Pratten, & Nguyen Tran Lam, 1999). The interparticle forces, especially those in high-concentration suspensions, are usually approximated within the framework of Kynch's theory (Kynch, 1952), by multiplying the Stokes velocity of the particles by an empirical factor, which is a function of local volumetric solid fractions only and is commonly referred to as hindered

* Corresponding author. Tel./fax: +86-22-2740-6590.
E-mail address: ysun@tju.edu.cn (Y. Sun).

0009-2509/03/$ - see front matter © 2003 Elsevier Science Ltd. All rights reserved.
doi:10.1016/S0009-2509(02)00656-5

settling function (HSF) or drag law (Masliyah, 1979; Davis & Gecol, 1994; Bürger & Tory, 2000). Although analytical formulae for the interaction between pairs of rigid spherical particles on the mean velocity of each species have been given by Batchelor (Batchelor, 1982) and evaluated numerically by Batchelor and Wen (Batchelor & Wen, 1982), these formulae are restricted to dilute suspensions and, as has been pointed out by those authors, are likely to be applicable to a system of two species of particles. The empirical approach to particle–particle interaction is therefore dominant in previous studies. Many HSFs for mono- and polydisperse suspensions have been proposed (Masliyah, 1979; Patwardhan & Tien, 1985; Khan & Richardson, 1989; Davis & Gecol, 1994), and some of them have proven to be capable of describing sedimentation and fluidization of bidisperse suspensions (Biesheuvel, Verweij, & Breedveld, 2001).

Unlike the artificial suspensions used in many studies containing only two to three particle species, most real suspensions encountered in practice, such as the adsorbent-liquid suspension in EBA, contain particles with continuous particle size and density distributions. However, only a few researchers have paid their attention to particles with a continuous particle size distribution (PSD) (Greenspan & Ungarish, 1982; Shih, Gidaspow, & Wasan, 1987; Davis & Hassen, 1988; Kumar, Pirog, & Ramkrishna, 2000). Many hypotheses concerning polydisperse sedimentation have been proposed and documented in literature, but most of them have yet to be confirmed by ample experimental evidences that are unavailable at present because of the tremendous difficulty in performing controlled experiments with polydisperse suspensions.

The purpose of this work is to analyze the settling behavior of two commercial gel-type spherical adsorbents, i.e. Sepharose CL-6B and Streamline SP. The particle size distributions of these beads are broader than those reported in previous publications, so the suspensions containing these beads bear more similarity to real suspensions. In fact, Streamline-based adsorbents are currently the most popular packing materials for EBA that is being more and more frequently used in food and pharmaceutical industries. To our knowledge, suspensions like these have not been studied before. Thus, this study is conducted to give an insight into the batch sedimentation behavior of highly polydisperse suspensions as well as to provide preliminary knowledge of the hydrodynamics of EBA. A mathematical model is generated to describe the sedimentation process of the beads. The model is embedded in the appropriate mathematical framework, i.e. in the form of partial differential equations, and solved numerically with a newly developed high-resolution shock-capturing technique. To date, this approach has only been applied to systems with low degrees of polydispersity (two to three particle species) (Bürger, Fjelde, Höfler, & Hvistendahl Karlsen, 2001; Berres, Bürger, Karlsen, & Tory, 2002), and our goal is to validate its applicability to systems consisting of more particle species (the number of species in this work is 35). It should be emphasized that the approach we adopted is more rigorous than the approximate one used by some other researchers (see, for example, Davis & Hassen, 1988). Theoretical calculations are compared with experiments to corroborate the model.

2. Theory

2.1. Conservation equations

In this article, we consider an initially homogeneous suspension consisting of a fluid and N species of spherical particles that have the same density ρ but differ in diameter. The particle species are numbered in descending order by their diameters, so that $d_1 > d_2 > \cdots > d_N$. The sedimentation of these particles is described by low-Reynolds-number hydrodynamics, where inertia, Brownian motion and colloidal forces are all negligible. Let u_i and ϕ_i denote the settling velocity and local volumetric fraction of species i, respectively. The following N scalar equations can be derived from the mass balance of the particles,

$$\frac{\partial \phi_i}{\partial t} + \frac{\partial f_i}{\partial x} = 0, \quad i = 1, 2, \ldots, N, \tag{1}$$

where f_i is the flux density function of species i, i.e.

$$f_i(\phi_1, \ldots, \phi_N) = \phi_i u_i(\phi_1, \ldots, \phi_N). \tag{2}$$

If the sedimentation takes place in a suspension of height H, and all the species are evenly distributed at the beginning, then the following initial and boundary conditions for Eq. (1) hold,

$$\phi_i = \phi_{i,0}, \quad t = 0,\ 0 < x < H, \tag{1a}$$

$$f_i = 0, \quad x = 0,\ t > 0, \tag{1b}$$

$$f_i = 0, \quad x = H,\ t > 0. \tag{1c}$$

2.2. Hindered settling functions

The common practice in predicting the settling velocity of solid particles is to define HSFs based either on u_i, the velocity of species i relative to the suspension, or on u_i^s, the slip velocity of species i relative to the fluid. In the former case, one has

$$u_i = h_i\, u_{i,0}, \tag{3}$$

where $u_{i,0}$ is the settling velocity of species i at infinite dilution ($\phi = \sum_{i=1}^{N} \phi_i \to 0$). If the container is sufficiently large to make the wall effect negligible, $u_{i,0}$ will be the same as $u_{i,0}^{\infty}$, the velocity of an isolated particle in an infinite medium, and can be calculated from Stokes' equation:

$$u_{i,0} = u_{i,0}^{\infty} = \frac{d_i^2(\rho - \rho_f)g}{18\mu_f}. \tag{4}$$

If the wall effect cannot be neglected, then Eq. (4) must be corrected by a factor (Khan & Richardson, 1989)

$$u_{i,0} = u_{i,0}^{\infty}[1 - 1.15(d_i/D)^{0.6}]$$

$$= \frac{d_i^2(\rho - \rho_f)g}{18\mu_f}[1 - 1.15(d_i/D)^{0.6}]. \quad (5)$$

There are many choices for h_i, and those proposed by Batchelor (Batchelor, 1982) (denoted $h_{i,B}$) and Davis and Gecol (Davis & Gecol, 1994) (denoted $h_{i,DG}$) are given below.

$$h_{i,B} = 1 + \sum_{j=1}^{N} S_{ij}\phi_j, \quad (6)$$

$$h_{i,DG} = (1-\phi)^{-S_{ii}}\left(1 + \sum_{j=1}^{N}(S_{ij} - S_{ii})\phi_j\right). \quad (7)$$

Eq. (6) is applicable in the dilute limit only, while Eq. (7) is a well-defined HSF for the whole range of concentrations from the dilute limit up to the packed bed.

In the latter case where HSFs are based on the slip velocity, the expression of u_i is not as straightforward as in the former case. The general form of different expressions follows Masliyah's derivation for batch sedimentation (zero net volumetric velocity of the suspension) (Masliyah, 1979).

$$u_i = h_i^s u_{i,0}\frac{\rho_i - \rho_s}{\rho_i - \rho_f} - \sum_{i=1}^{N}\phi_i h_i^s u_{i,0}\frac{\rho_i - \rho_s}{\rho_i - \rho_f}, \quad (8)$$

where ρ_s is the density of the suspension defined by

$$\rho_s = (1-\phi)\rho_f + \sum_{i=1}^{N}\phi_i\rho_i. \quad (9)$$

For equidensity particles, Eq. (8) reduces to

$$u_i = (1-\phi)\left(h_i^s u_{i,0} - \sum_{j=1}^{N}\phi_j h_j^s u_{j,0}\right). \quad (10)$$

The most commonly used HSFs proposed by Masliyah (Masliyah, 1979) ($h_{i,M}^s$) and Patwardhan and Tien (Patwardhan & Tien, 1985) ($h_{i,PT}^s$) are expressed respectively as follows:

$$h_{i,M}^s = (1-\phi)^{n-2} \quad (11)$$

$$h_{i,PT}^s = \left(1 - \left(1 + \frac{d_\varepsilon}{d_i}\right)^{-3}\right)^{n-2},$$

$$d_\varepsilon = \frac{\sum_{j=1}^{N} d_j\phi_j}{\phi}(\phi^{-1/3} - 1). \quad (12)$$

In this work, Masliyah's HSF (Eq. (11)) is adopted to simulate the dynamic behavior of particle settling because it has proven to be able to successfully describe the sedimentation and fluidization of binary systems in various experimental situations (Biesheuvel, Verweij, & Breedveld, 2001). More importantly, recent analysis by Berres et al. (2002) showed that the Masliyah model (i.e., Eq. (1) with the Masliyah HSF) was always hyperbolic for equidensity particles with arbitrary numbers of particle species and particle size distributions. This feature ensures that any information in the system travels at finite speed, and that the problem is well posed. On the contrary, the Davis and Gecol model (Eq. (7)) gives rise to unphysical instability (non-hyperbolicity) regions of Eq. (1) (Bürger, Karlsen, Tory, & Wendland, 2002), and hence is not evaluated in this work. The Patwardhan and Tien model is not tested either, for its stability has not been validated yet.

In all the simulations to be mentioned below, the exponent n in Eq. (11) is set at 4.65 following Wallis (Wallis, 1969), and the function is cut at a maximum solid concentration, $\phi_{\max}$, of 0.6 in a way similar to those reported in previous publications (Concha, Lee, & Austin, 1992; Bürger, Concha, Fjelde, & Hvistendahl Karlsen, 2000; Bürger et al., 2001). The choice of $\phi_{\max}$ is based on the measured interstitial voidage of packed spherical beads, which is 0.4 for both the Sepharose (Boyer & Hsu, 1992) and Streamline beads (Willoughby, Hjorth, & Titchener-Hooker, 2000; Bruce & Chase, 2001).

2.3. Numerical method

Due to the nonlinear nature of the flux density function (Eq. (2)), the solution of the hyperbolic system of conservation laws (Eq. (1)) is discontinuous even with smooth initial conditions. The appearance of discontinuities requires great efforts to solve the conservation equations with existing numerical schemes such as the method of characteristics (Shih, Gidaspow, & Wasan, 1986), and many researchers turn to approximate solutions by assuming a series of finite zones in which the concentrations and settling velocities of each particle species are constant (Davis & Hassen, 1988; Stamatakis & Tien, 1988). With the development of modern difference schemes, however, this problem has become less difficult than it used to be. In recent publications, Bürger and co-workers (Bürger et al., 2000, 2001) reported the solution of conservation equations with one of the latest modern entropy-satisfying shock-capturing central difference scheme for nonlinear systems, which was originally developed by Nessyahu and Tadmor (Nessyahu & Tadmor, 1990) and then modified by Kurganov and Tadmor (Kurganov & Tadmor, 2000). They compared their simulation results with the settling data of a bidisperse suspension, and found good agreement between them.

Encouraged by the success of Bürger and co-workers, we employed the above-mentioned difference scheme in our work, too. However, the difference was that we chose the semi-discrete scheme (Kurganov & Tadmor, 2000) rather than the fully discrete scheme used by Bürger and co-workers (Bürger et al., 2001). A program was written on the platform of Matlab 5.3. The ordinary differential equations (ODE) obtained by semi-discrete differencing

were integrated numerically with ODE23, a low order ODE solver embedded in Matlab 5.3. Comparison between our simulation results and those of Bürger et al. for the bidisperse system (Bürger et al., 2001) indicated that the program works correctly (data not shown).

In the calculations shown below, we set M, the number of grid cells for the spatial discretization, at 200 (the total spatial length was 20 cm) to make a numerical compensation for particle diffusion (see Section 5). The number of particle species, N, was set at 35; further increase in this number had little influence on the simulation results. Under these conditions, the running time of the program on a personal computer (Pentium III 750 MHz, 64 M RAM) ranged from 5 to 8 min for one batch.

3. Materials and methods

3.1. Materials

Agarose-based spherical particles under the commercial names of Sepharose CL-6B and Streamline SP, respectively, were purchased from Amersham Pharmacia Biotech (Uppsala, Sweden). Since Sepharose CL-6B beads were semi-transparent, they were dyed with Cibacron blue F3G-A (Sigma, St. Louis, MO, USA) to facilitate visual observation. A commonly used dying procedure (Xue & Sun, 2001) was employed, yielding a dye density of 10 μmol/ml in the beads measured by the acid digestion method (He, Gan, & Sun, 1997). Streamline SP beads were opaque because of the quartz granules in them and therefore were used as received. The particle size distributions of the two kinds of beads were measured with a Mastersizer 2000 unit (Malvern Instruments Ltd., UK). A 25-ml pycnometer was used to measure the beads' hydrated densities.

The fluid for the dyed Sepharose CL-6B was deionized water. For the dense Streamline SP particles, aqueous glycerol solutions were employed to slow down the sedimentation process and hence make easier the recording of experimental data. Three glycerol solutions of different concentrations (45%, 65% and 75%, w/w) were used in the experiments. The densities and viscosities of all the fluids at 20°C along with the densities of the beads in these fluids are given in Table 1.

3.2. Apparatus

A light-extinction principle was employed to detect particle concentration in the suspension at different time and positions, similar to that reported by Davis and Hassen (Davis & Hassen, 1988). To do this, the sampling chamber (12.5 × 9.0 × 12.0 cm, length by width by height) of a spectrophotometer (Type 9110, Rayleigh Optical Instrument Co., Beijing, China) was replaced with a taller one (12.5 × 9.0 × 70.0 cm), and a larger holder was equipped in it. The holder was specially designed for a customized glass cuvette (inside dimension 25 cm high and 1.0 cm by 1.0 cm in cross-section) and could move vertically. In one sidewall of the chamber was a 1.0 cm wide by 0.5 cm high slit. A light beam could enter through the slit into the chamber, pass the cuvette containing particle suspensions, and reach the photodiode in the opposite wall. The wavelength of the beam was adjustable within the range from 180 to 1000 nm. An A/D converter converted the intensity of the transmitted light into digital data acquired by a personal computer. The maximum sampling rate was 10 data points per second.

3.3. Experimental procedure

All the sedimentation experiments were conducted at 20.0 ± 0.5°C. The beads were firstly allowed to immerse in their corresponding fluid for 12 h in a graduated cylinder, resulting in a tightly packed bed. The total volume of the beads was then calculated from the bed volume, which was indicated by the scale of the cylinder, and the interstitial voidage of packed spherical beads (0.4, see above). The beads were then re-suspended by agitation and a definite volume of the fluid was added to give a suspension of known solid volumetric fraction. The suspension was agitated vigorously to eliminate as far as possible inhomogeneities in it, and 20 ml of it was poured into the customized cuvette that had been placed in the holder beforehand. Convective motion of the suspension in the cuvette was damped out by the suspension viscosity in a few seconds. At the cessation of this motion, sampling of the transmitted light intensity was started, and the time course of absorbance decline was recorded. When the absorbance dropped to zero, the sampling was stopped, which marked the end of the experimental procedure for one batch. The monitoring position,

Table 1
Physical properties of fluids and beads at 20°C

Fluid name	ρ_f (g/cm^3)[a]	μ_f (mPa s)[a]	ρ_{Sep} (g/cm^3)[b]	ρ_{Str} (g/cm^3)[b]	$\rho_{Str,cal}$ (g/cm^3)
Water	0.99823	1.005	1.03	1.18	
45% glycerol	1.11280	4.715	ND[c]	1.28	1.28
65% glycerol	1.16750	15.54	ND	1.34	1.33
75% glycerol	1.19485	36.46	ND	1.35	1.35

[a]From (Weast, 1988).
[b]Measured with a 25-ml pycnometer.
[c]Not determined.

Table 2
Particle size distributions of sepharose and streamline beads

Beads type	Std. sieve range	d_{43} (σ) (μm)	$\sigma/d_{43}(-)$	d_{32} (μm)
Sepharose CL-6B				
Unclassified		89 (26)	0.29	82
Fraction 1	−300	56 (13)	0.24	53
Fraction 2	−200 + 300	72 (18)	0.25	68
Fraction 3	+200	96 (25)	0.26	90
Streamline SP				
Unclassified		107 (37)	0.35	203
Fraction 1	−100	67 (21)	0.31	146
Fraction 2	+100	108 (36)	0.33	209

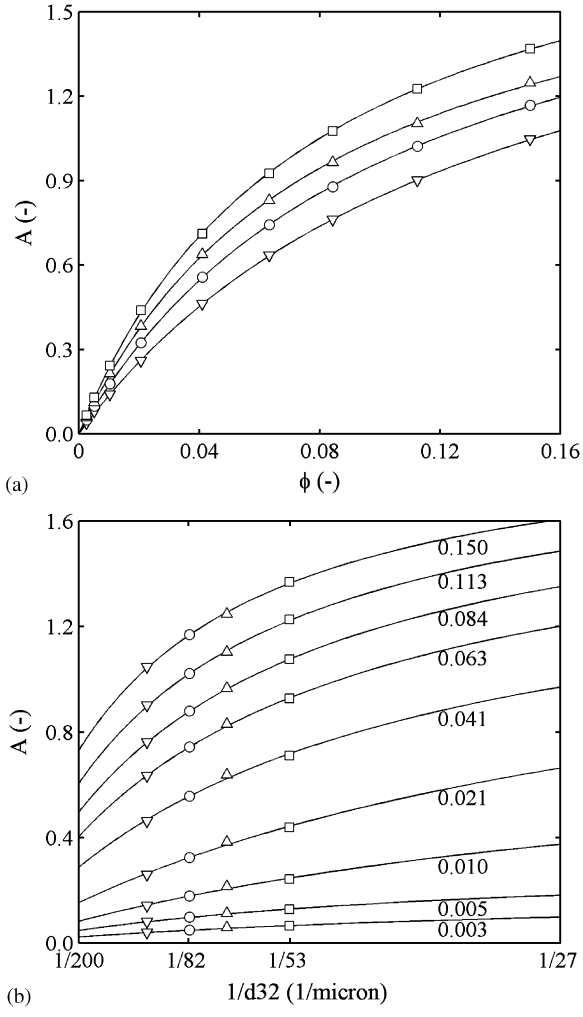

Fig. 1. Initial absorbance of Sepharose particle suspensions as a function of the particles' volumetric fraction and surface-weighted mean diameter. d_{32} values are (□) 53, (△) 68, (○) 82 and (▽) 90 μm. Numbers in (b) are concentration values of the iso-concentration lines.

i.e. the distance between the top of the suspension and the light beam, was then adjusted by moving the holder, and the above procedure was repeated for a new batch.

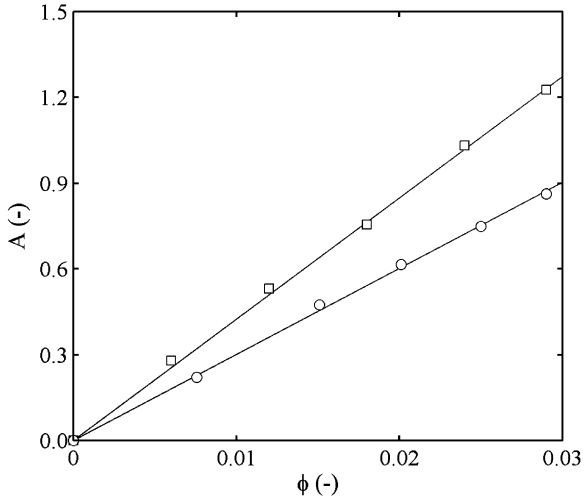

Fig. 2. Initial absorbance of Streamline particle suspensions as a function of the particles' volumetric fraction and surface-weighted mean diameter. The fluid is 75% aqueous glycerol solution. (□) $d_{32} = 146$ μm, slope = 0.428; (○) $d_{32} = 209$ μm, slope = 0.301.

4. Results

4.1. Variation of particle density with fluids

The porous nature of the gel-type beads gives rise to an interesting phenomenon, i.e. the beads' hydrated density depends positively on the density of the fluid (see Table 1). Based on the data given in Table 1, the density of Streamline SP beads in 45%, 65% and 75% glycerol solutions were calculated from the following equations,

$$\rho_{\mathrm{Str,cal}} = \phi_{\mathrm{quartz}} \times \rho_{\mathrm{quartz}} + (1 - \phi_{\mathrm{quartz}} - \varepsilon_{\mathrm{Str}}) \times \rho_{\mathrm{agarose}} + \varepsilon_{\mathrm{Str}} \times \rho_f, \quad (13)$$

$$\phi_{\mathrm{quartz}} = \frac{\rho_{\mathrm{Str},w} - \rho_{\mathrm{Sep},w}}{\rho_{\mathrm{quartz}} - \rho_{\mathrm{Sep},w}}, \quad (14)$$

$$\varepsilon_{\mathrm{Str}} = (1 - \phi_{\mathrm{quartz}}) \times \varepsilon_{\mathrm{Sep}}, \quad (15)$$

$$\rho_{\mathrm{agarose}} = \frac{\rho_{\mathrm{Sep},w} - \varepsilon_{\mathrm{Sep}} \times \rho_w}{1 - \varepsilon_{\mathrm{Sep}}}, \quad (16)$$

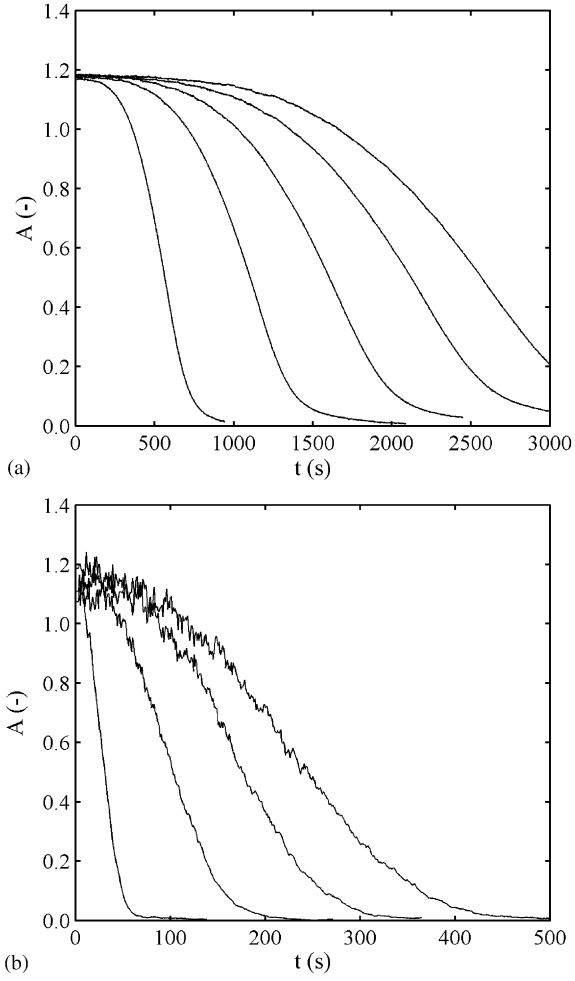

Fig. 3. Typical raw absorbance data obtained from batch sedimentation. (a) Sepharose beads in water, $\phi_0 = 0.156$, settling distances are 2, 4, 6, 8 and 10 cm (from left to right). (b) Streamline beads in 45% glycerol solution, $\phi_0 = 0.021$, settling distances are 2, 6, 10 and 14 cm (from left to right).

where ε_{Sep} is 0.94 according to the agarose content (6%) in the beads, and ρ_{quartz} is 2.6 g/cm^3 (Weast, 1988). The calculated volumetric fraction of quartz in Streamline SP is 0.096, and the voidage of Streamline SP beads is given at 0.86. Densities of Streamline SP beads calculated from Eq. (13) are also listed in Table 1. The good agreement between the calculated and measured densities justifies the reliability of these data.

It should be noted that the particle densities in Table 1 are average values of many beads. For the equidensity Sepharose CL-6B, the value represents the density of any single bead. For Streamline SP that consists of crosslinked agarose and quartz granules, there exists a narrow particle density distribution (PDD) (Bruce & Chase, 2001). At present it seems very difficult to determine the PDD and its relation with the PSD by available techniques, so the average density is used in the mathematical model (Eq. (5)) without considering the PDD.

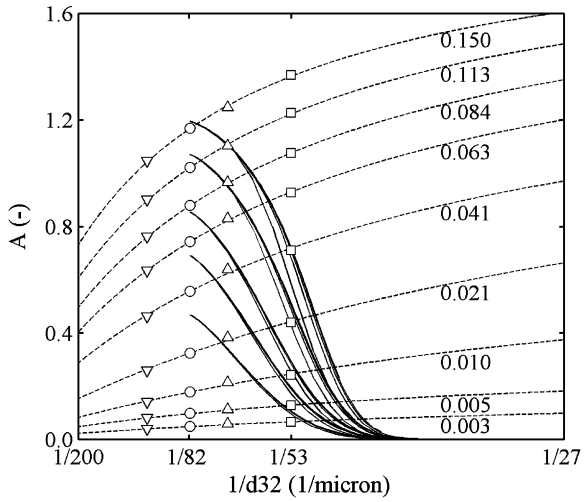

Fig. 4. Illustration of two-dimensional interpolation/extrapolation procedure used in calculating the volumetric fractions (solid lines) of Sepharose beads suspension with known absorbance values and mean particle diameter. The symbols and dashed lines are the same as shown in Fig. 1. For experimental details see the legend to Fig. 5.

4.2. Calibrations for absorbance vs. particle concentration and diameter

In this paper, the solid concentration is expressed by the volumetric fraction of the solid in the solid–liquid suspension. Determined by the measurement range of the spectrophotometer and the opacity of the beads, the maximum measurable solid concentrations are restricted to 0.16 for Sepharose CL-6B and 0.03 for Streamline SP under a wavelength of 980 nm. The shorter the wavelength, the smaller the maximum concentrations. In this article, the wavelength was set at 980 nm. Sedimentations at five Sepharose concentrations (0.033–0.156) and one Streamline SP concentration (0.021) were investigated.

According to Beer's law, the light absorbance of a particle suspension is proportional to the total cross-sectional area of particles present in the beam. For polydisperse suspensions, one has

$$A = k' \sum_{i=1}^{N} n_i d_i^2 = k' \sum_{i=1}^{N} n_i d_i^2 \frac{\sum_{i=1}^{N} n_i d_i^3}{\sum_{i=1}^{N} n_i d_i^3}$$

$$= k\phi \left(\frac{\sum_{i=1}^{N} n_i d_i^3}{\sum_{i=1}^{N} n_i d_i^2} \right)^{-1} = k \frac{\phi}{d_{32}}, \qquad (17)$$

where k' and k are proportionality constants, and N is the number of particle species in the beam. However, as has been pointed out by Davis and Birdsell (Davis & Birdsell, 1988), Eq. (17) is often violated by multiple scattering effects and is only valid at low solid concentrations ($\phi \leqslant 0.02$) for suspensions with unmatched particle and fluid refractive indices. In other words, k is no longer a constant for the Sepharose particle concentrations studied

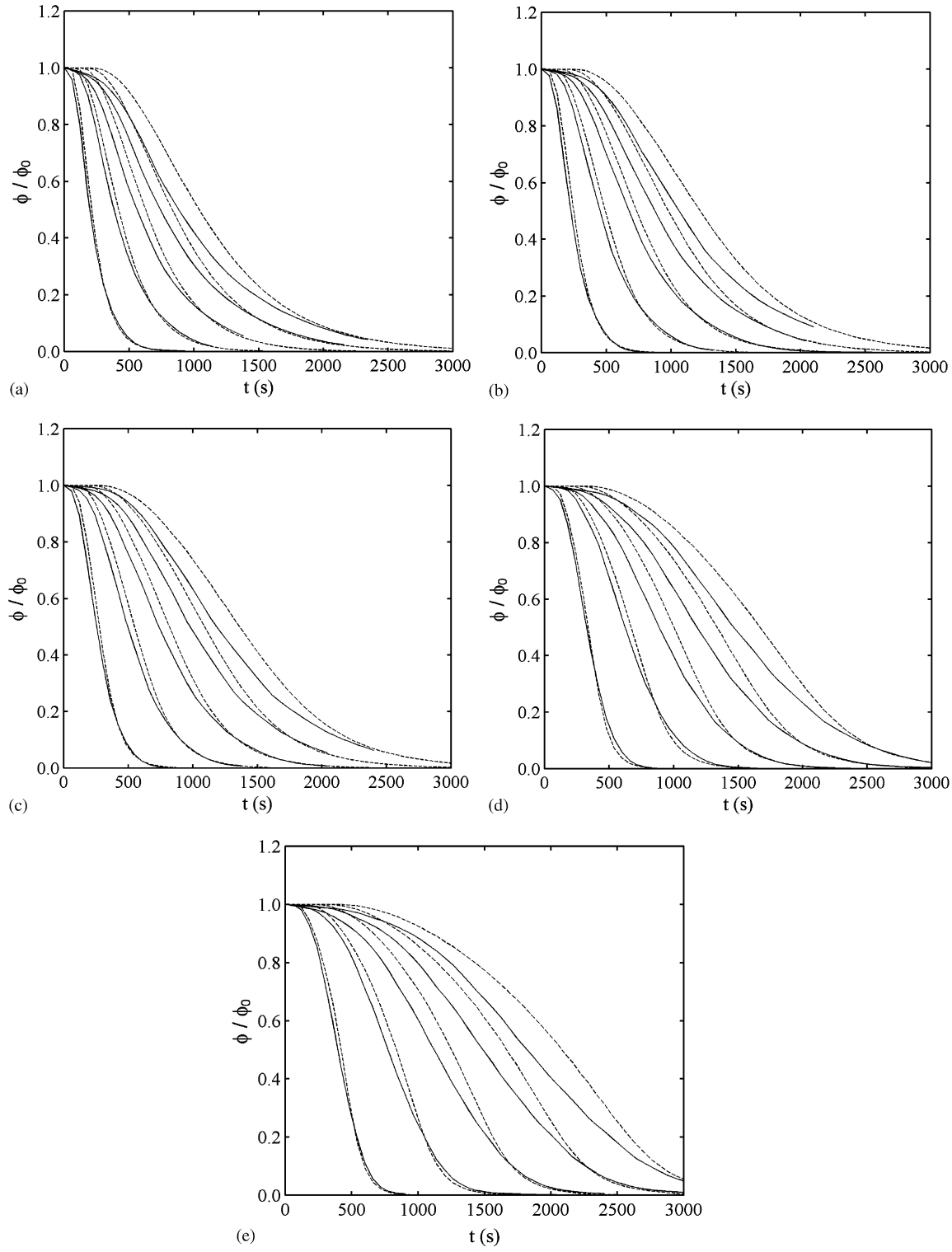

Fig. 5. Experimental (solid lines) and calculated (dashed lines) volumetric fractions of Sepharose beads. Initial solid concentrations in the suspensions are (a) 0.033, (b) 0.056, (c) 0.080, (d) 0.122 and (e) 0.156. Settling distances are 2, 4, 6, 8 and 10 cm for both the solid and dashed lines (from left to right).

in this work. So it is necessary to determine the relation of A with ϕ and d_{32} experimentally. Toward this end, a portion of Sepharose beads was classified with 300- and 200-mesh standard sieves, yielding three fractions. The PSDs of these particle fractions are of lognormal type and are characterized by the parameters listed in Table 2.

Fig. 1a shows the initial absorbance of suspensions prepared with unclassified and classified Sepharose beads at

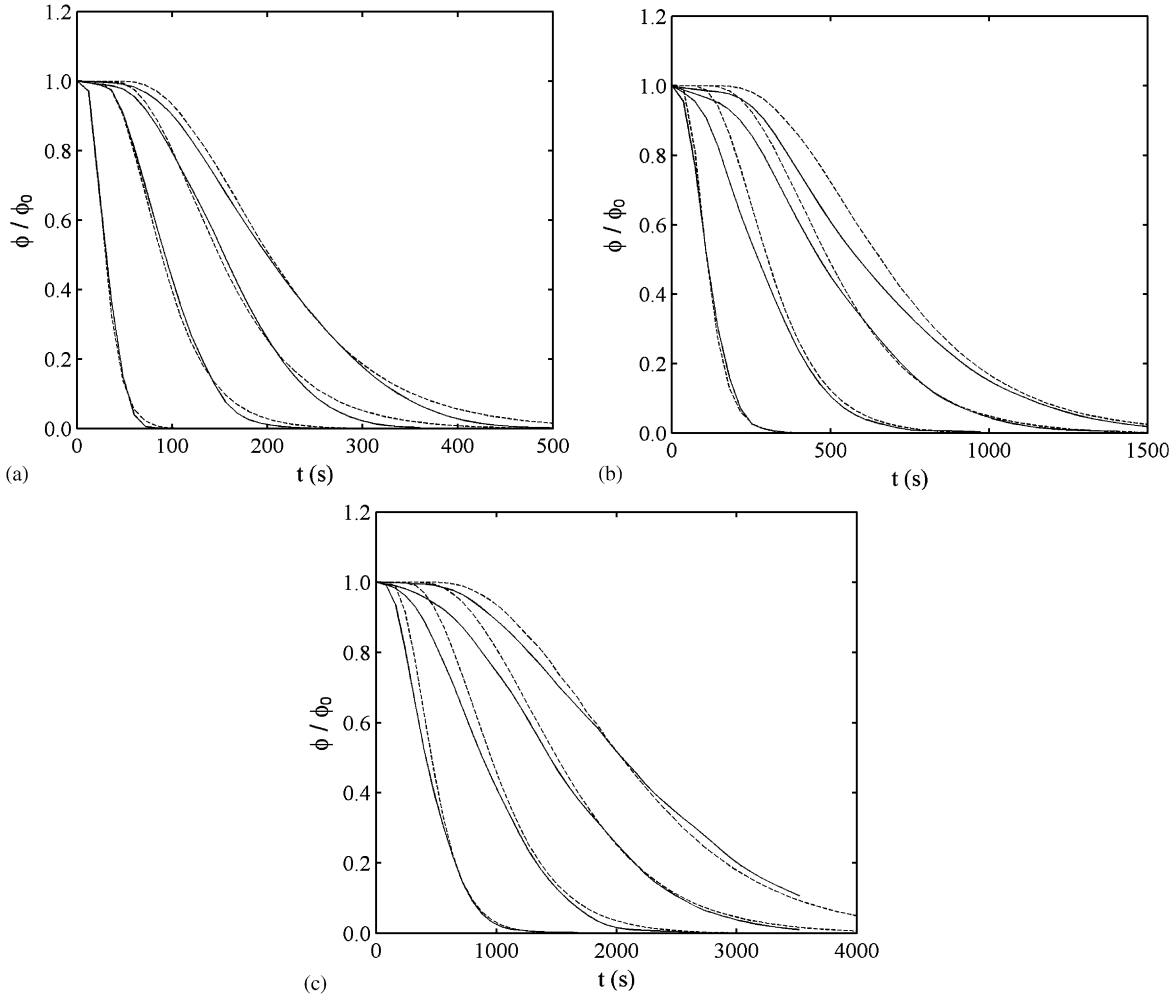

Fig. 6. Experimental (solid lines) and calculated (dashed lines) volumetric fractions of Streamline beads dispersed in (a) 45%, (b) 65% and (c) 75% aqueous glycerol solutions. Initial solid concentrations in the suspensions are fixed at 0.021. Settling distances are 2, 6, 10 and 14 cm for both the solid and dashed lines (from left to right).

different solid concentrations. The scattered symbols in the figure are averages of three replicates, and the standard deviations from these replicates are less than 1.0%, indicating a good reproducibility of the results. Fig. 1b, which is redrawn from Fig. 1a, clearly shows that the iso-concentration lines remain straight at low solid concentrations but bend when the concentration exceeds 0.02. Although the measurements were conducted with only four different d_{32} values, the results were interpolated and extrapolated to cover the whole range of Sepharose particle diameter from 27 to 200 μm. As will be seen later, the interpolation and extrapolation are needed to compare simulation results with experimental data.

Fig. 2 shows the A–ϕ curves of Streamline SP beads obtained in a way similar to those of Sepharose beads. A 100-mesh standard sieve was used to separate Streamline beads into two fractions. The slopes of the two straight lines in Fig. 2 are 0.428 and 0.301, respectively, for the small ($d_{32} = 146$ μm, see Table 2) and large ($d_{32} = 209$ μm) fractions. From Eq. (17) one has,

$$k = \frac{A}{\phi} d_{32}. \tag{18}$$

The k values calculated from Eq. (18) are 62.5 for the small fraction and 62.9 for the large one, which indicates that for Streamline beads Eq. (17) is applicable to correlate A with ϕ and d_{32} within the range $\phi \leqslant 0.03$. The k is set at 62.7 μm in the following sections.

4.3. Comparison between experimental and theoretical results

Fig. 3 shows typical absorbance data for Sepharose and Streamline beads with different settling distances. Due to the random noise that arises from the statistical fluctuation of beads number in the light beam, the curves are not absolutely smooth. The smaller the beads number, the more intense the fluctuation. This explains why the noise in

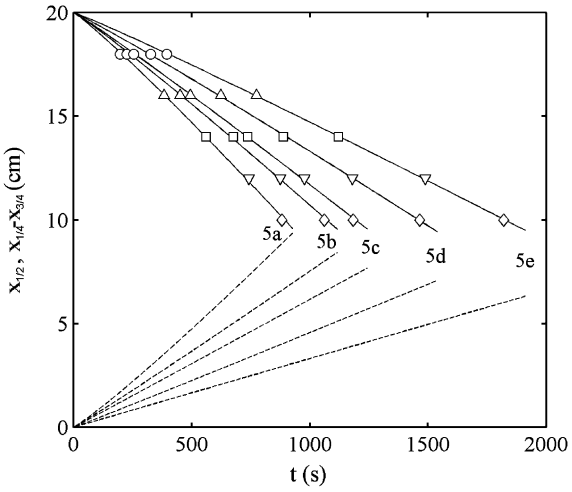

Fig. 7. Settling and spreading of the interface at the top of the suspensions containing Sepharose beads. Solid lines show the trajectories of the iso-concentration plane $\phi/\phi_0 = 1/2$ ($x_{1/2}$ vs. t). Dashed lines depict the distances between the two iso-concentration planes $\phi/\phi_0 = 1/4$ and $\phi/\phi_0 = 3/4$ ($(x_{1/4}–x_{3/4})$ vs. t). As indicated in the figure, these lines correspond to Figs. 5a–e, respectively. Settling distances are (◯) 2 cm, (△) 4 cm, (□) 6 cm, (▽) 8 cm, and (◇) 10 cm.

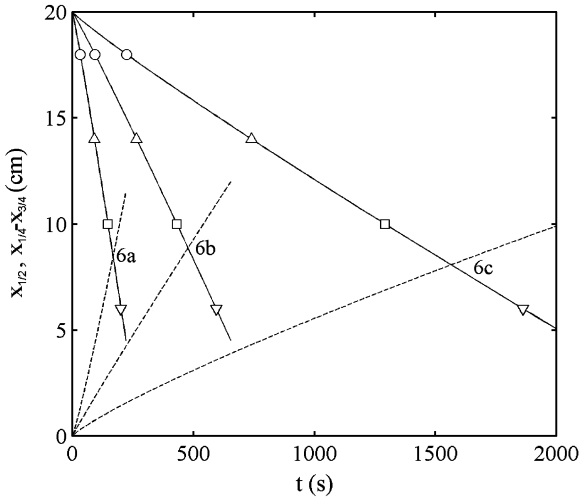

Fig. 8. Settling and spreading of the interface at the top of the suspensions containing Streamline beads. Solid lines show the trajectories of the iso-concentration plane $\phi/\phi_0 = 1/2$ ($x_{1/2}$ vs. t). Dashed lines depict the distances between the two iso-concentration planes $\phi/\phi_0 = 1/4$ and $\phi/\phi_0 = 3/4$ ($(x_{1/4}–x_{3/4})$ vs. t). As indicated in the figure, these lines correspond to Figs. 6a–c, respectively. Settling distances are (◯) 2 cm, (△) 6 cm, (□) 10 cm, and (▽) 14 cm.

Fig. 3b, where the diameter of the beads is larger but the concentration is lower, is more significant than that in Fig. 3a. To eliminate the random noise and to make the comparison of data from different batches easier, all the raw data were smoothed and normalized. A cubic smoothing spline function, CSAPS, provided by Matlab 5.3 was used in data smoothing. Data after these treatments are compared with theoretical calculations.

Solution of Eq. (1) yielded the volumetric fractions of each particle species as functions of time and settling distances. To make reasonable comparisons between simulated and experimental results, we converted measured light absorbance data into particle volume fractions with the aid of the aforementioned calibration curves (Fig. 1, for Sepharose beads) or Eq. (17) (for Streamline beads). Simulation results under the same conditions were utilized to provide local average particle diameters needed for such a conversion. For Sepharose beads, the conversion involves a two-dimensional interpolation/extrapolation procedure based on the data shown in Fig. 1, which is elucidated in Fig. 4. We know from this figure that extrapolation along the iso-concentration lines is linear in most cases owing to the low solid concentrations at which it happens, which ensures the accuracy and reliability of the extrapolated data.

It can be seen from Figs. 5 and 6 that the agreements between experimental (solid lines) and simulation results (dashed lines) are generally good for both Sepharose and Streamline beads. Discrepancies occurring at the upper and middle parts of the ϕ–t curves are most likely caused by particle diffusion and initial inhomogeneities in the suspensions. The diffusion mechanism involved in particle sedimentation, termed "self-induced hydrodynamic diffusion" by Davis and Hassen after G. K. Batchelor (Davis & Hassen, 1988), arises from the fluctuations in particle settling velocities around their mean and reflects hydrodynamic interactions between solid particles. The hydrodynamic diffusion is strong at the beginning of a batch sedimentation procedure, when the particle concentration gradient is large at the top of the suspension. This phenomenon may lead to disagreements between the solid and dashed lines in Figs. 5 and 6, especially in their upper parts, if it is not accurately defined in the model. The choice of particle diffusivities will be further discussed below. From Fig. 5 we know that the discrepancies in the upper part of the ϕ–t curves decrease from low (Fig. 5a) to high concentrations (Fig. 5e), which is consistent with the observation that particle diffusion depends negatively on particle concentrations within certain concentration range (Davis & Hassen, 1988). This consistency may serve as an evidence of the impact of particle diffusion.

Besides the particle diffusion, initial inhomogeneities in the suspensions are also an important reason for the disagreements between experimental data and theoretical calculations. Although great cautions have been taken to eliminate as completely as possible any initial nonuniformity in the suspensions, it is extremely difficult to achieve a truly even dispersion of polydisperse particles in a fluid (Bürger et al., 2001). So a macroscopically homogeneous suspension without any visible particle segregations may actually contain many particle clusters when observed from a microscopic point of view. Solid concentration in these clusters is higher than in their surroundings, so the clusters settle more quickly than single particles and act as if they were new

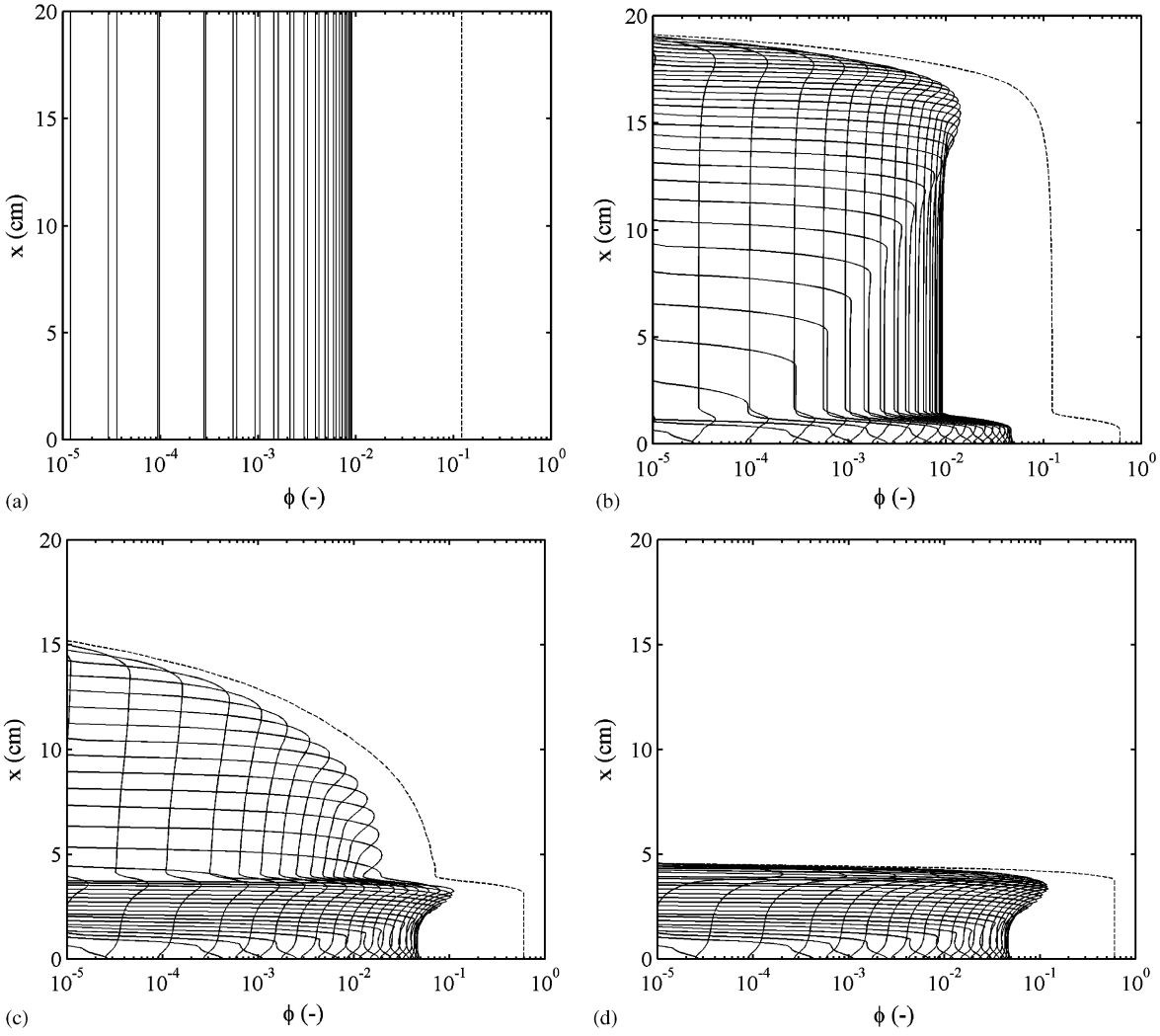

Fig. 9. Concentration profiles of Sepharose beads in water. The number of particle species is 35. The dashed line in the figure indicates the total volumetric fraction of all the species, whose initial value is 0.122. Snapshots are taken at (a) $t = 0$ min, (b) $t = 10$ min, (c) $t = 40$ min, and (d) $t = 120$ min.

particle species whose diameters exceed the largest particle diameter in the suspension, which results in a faster decrease in absorbance response. Since the model does not account for the inhomogeneities in the suspension, the discrepancies in the middle part of the ϕ–t curves rise gradually from Fig. 5a ($\phi_0 = 0.033$) to Fig. 5e ($\phi_0 = 0.156$), through which the size and number of the clusters increase with the initial solid concentration of the suspension.

To further characterize the falling speed and spreading of the interface at the top of the suspensions, Figs. 5 and 6 are recast into Figs. 7 and 8, respectively, by tracing the movement of certain iso-concentration planes in the suspension. Three planes with local particle concentrations being 1/4, 1/2 and 3/4 of the initial value are trailed in this work, and their positions in the suspension are denoted $x_{1/4}$, $x_{1/2}$, and $x_{3/4}$, respectively. Two lines are obtained for each sub-figure in Figs. 5 and 6: one is $x_{1/2}$ vs. t, which characterizes the average settling velocity of the interface; the other is $(x_{1/4}$–$x_{3/4})$ vs. t, which quantifies the spreading of the interface. All the lines shown in Figs. 7 and 8 are linear (or almost linear), which means that the average settling velocity of the interface is constant and the spreading of the interface is proportional to the settling time. In addition, Fig. 7 also clearly shows the hindered settling effect, which leads to the decrease in the slope of the solid lines (absolute value) with increasing particle concentrations.

5. Discussion

Davis and Hassen (Davis & Hassen, 1988) studied the spreading of the interface at the top of a slightly polydisperse glass beads suspension and found that the beads' diffusion coefficients varied with the initial solid concentrations and reached their maxima at certain concentrations. The diffusivities obtained within the concentration range

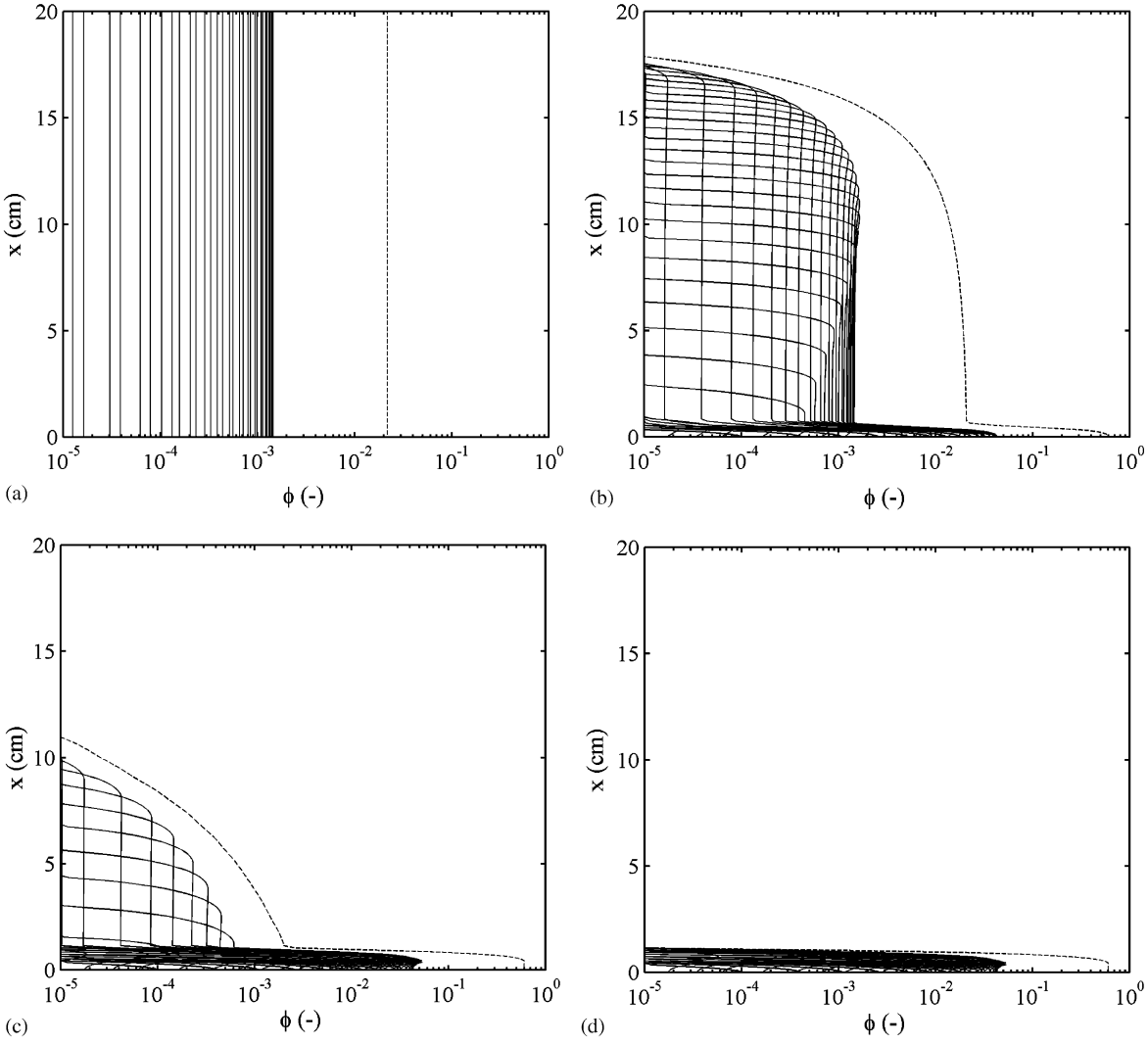

Fig. 10. Concentration profiles of Streamline beads in 45% glycerol solution. The number of particle species is 35. The dashed line in the figure indicates the total volumetric fraction of all the species, whose initial value is 0.021. Snapshots are taken at (a) $t = 0$ min, (b) $t = 2$ min, (c) $t = 8$ min, and (d) $t = 20$ min.

$0.005 \leqslant \phi \leqslant 0.15$ were on the order of 10^{-7} m^2/s, and the ratio of the diffusivities to their corresponding average settling velocities was on the order of 10^{-3} m.

At present it is still difficult to accurately quantify the diffusivity with a well-defined mathematical correlation, so we did not add a diffusion term on the right-hand side of Eq. (1) in this work, though the numerical scheme employed can be applied to convection-diffusion equations in a straightforward manner (Kurganov & Tadmor, 2000). Instead, we adopted a relatively low spatial discretization degree ($M = 200$) to compensate the particle diffusion by numerical dissipation. Results calculated in this way have been compared with those from the convection-diffusion equations with a high spatial discretization degree ($M = 800$) and a constant ratio of diffusivity to velocity (1×10^{-3} m) for different particle species (data not shown), and a striking resemblance was found between them. Since the former approach is more economical in terms of computing time, it has been used in all the simulation processes to account for particle diffusion.

Figs. 9 and 10 depict theoretical particle concentration profiles in Sepharose and Streamline beads suspensions at different time. The accumulation of small particles near the supernatant-suspension interface can clearly be seen in Fig. 9, which is attributed to both the continuity of particle flux and the hindrance effect to particle settling. This phenomenon has become known as Smith effect (Smith, 1966). Due to the logarithmic scale, this effect appears less pronounced than it actually is. At a low solid concentration the hindrance effect is weak, so the accumulation in Fig. 10 is not as significant as in Fig. 9. Though the actual profiles may be different due to the initial inhomogeneities, these figures are nonetheless helpful because they provide a visual

illustration of hindered sedimentation in an ideal polydisperse suspension.

6. Conclusions

The sedimentation of two kinds of polydisperse agarose beads, Sepharose CL-6B and Streamline SP, were studied experimentally and theoretically. A light-extinction principle was used to measure the variation of solid concentration in the suspension with time and settling distance. A mathematical model consisting of the conservation equations of particles and Masliyah's hindered settling function was utilized to describe the sedimentation process. The simulation results are generally good when compared with experimental ones, justifying the soundness of the model in formulating the sedimentation of polydisperse particles. Disagreements appearing at the upper part of absorbance vs. time curves are attributed to initial inhomogeneities in the suspensions that are not considered in the model.

To further validate the correctness of the kinematical model employed in this work, new methods are desired for noninvasive, on-line measurement of not only the total solid concentration but also the concentrations of each particle species in the suspension. A more thorough comparison between experiments and theoretical predictions could be made if more details are known about the PSD in the suspension at any time and settling distance. Some techniques have been developed for this purpose by using high-frequency acoustic waves (Alba, Crawley, Fatkin, Higgs, & Kippax, 1999; Stolojanu & Prakash, 2001), which might be adopted in future work.

Notation

A	absorbance
d	particle diameter, μm or m
d_{32}	surface-weighted mean particle diameter, μm or m
d_{43}	volume-weighted mean particle diameter, μm or m
D	equivalent hydraulic diameter of the container, m
h	hindered settling function
H	height of the suspension, m
k, k'	proportionality constants, μm or m
M	number of grid cells for spatial discretization
N	number of particle species
t	time, s
x	spatial variable, m

Greek letters

ε	particle porosity
μ	viscosity, mPa s
ρ	density, kg/m^3
σ	standard deviation of particle diameter, μm or m
ϕ	volumetric fraction

Superscripts

s	slip velocity
∞	infinite container

Subscripts

0	initial state
i	ith particle species
f	fluid
s	suspension
Sep	Sepharose CL-6B
Str	Streamline SP
w	water

Acknowledgements

This work was supported by the National Natural Science Foundation of China (grant No. 20025617).

References

Alba, F., Crawley, G. M., Fatkin, J., Higgs, D. M. J., & Kippax, P. G. (1999). Acoustic spectroscopy as a technique for the particle sizing of high concentration colloids, emulsions and suspensions. *Colloids and Surfaces A: Physiochemical and Engineering Aspects*, *153*, 495–502.

Anspach, F. B., Curbelo, D., Hartmann, R., Garke, G., & Deckwer, W. -D. (1999). Expanded-bed chromatography in primary protein purification. *Journal of Chromatography A*, *865*, 129–144.

Batchelor, G. K. (1982). Sedimentation in a dilute polydisperse system of interacting spheres. Part 1. General theory. *Journal of Fluid Mechanics*, *119*, 379–408.

Batchelor, G. K., & Wen, C.-S. (1982). Sedimentation in a dilute polydisperse system of interacting spheres. Part 2. Numerical results. *Journal of Fluid Mechanics*, *124*, 495–528.

Batt, B. C., Yabannavar, V. M., & Singh, V. (1995). Expanded bed adsorption process for protein recovery from whole mammalian cell culture broth. *Bioseparation*, *5*, 41–52.

Berres, S., Bürger, R., Karlsen, K. H., & Tory, E. M. (2002). Strongly degenerate parabolic-hyperbolic systems modeling polydisperse sedimentation with compression. *Preprint* (*Available via http://www.math.ntnu.no/conservation/2002/025.html*).

Biesheuvel, P. M., Verweij, H., & Breedveld, V. (2001). Evaluation of instability criterion for bidisperse sedimentation. *A.I.Ch.E. Journal*, *47*(1), 45–52.

Boyer, P. M., & Hsu, J. T. (1992). Experimental studies of restricted protein diffusion in an agarose matrix. *A.I.Ch.E. Journal*, *38*, 259–272.

Bruce, L. J., & Chase, H. A. (2001). Hydrodynamics and adsorption behaviour within an expanded bed adsorption column studied using in-bed sampling. *Chemical Engineering Science*, *56*, 3149–3162.

Bürger, R., Concha, F., Fjelde, K.-K., & Hvistendahl Karlsen, K. (2000). Numerical simulation of the settling of polydisperse suspensions of spheres. *Powder Technology*, *113*, 30–54.

Bürger, R., Fjelde, K. -K., Höfler, K., & Hvistendahl Karlsen, K. (2001). Central difference solutions of the kinematic model of settling of polydisperse suspensions and three-dimensional particle-scale simulations. *Journal of Engineering Mathematics*, *41*, 167–187.

Bürger, R., Karlsen, K. H., Tory, E. M., & Wendland, W. L. (2002). Model equations and instability regions for the sedimentation of polydisperse suspensions of spheres. *Zeitschrift Fur Angewandte Mathematik und Mechanik*, *82*(10), 699–722.

Bürger, R., & Tory, E. M. (2000). On upper rarefaction waves in batch settling. *Powder Technology*, *108*, 74–87.

Cheung, M. K., Powell, R. L., & McCarthy, M. J. (1996). Sedimentation of noncolloidal bidisperse suspensions. *A.I.Ch.E. Journal*, *42*(1), 271–276.

Clemmitt, R. H., & Chase, H. A. (2000). Facilitated downstream processing of a histidine-tagged protein from unclarified *E. coli* homogenates using immobilized metal affinity expanded-bed adsorption. *Biotechnology and Bioengineering*, *67*, 206–216.

Concha, F., Lee, C. H., & Austin, L. G. (1992). Settling velocities of particulate systems: 8. Batch sedimentation of polydisperse suspensions of spheres. *International Journal of Mineral Processing*, *35*, 159–175.

Davis, R. H., & Birdsell, K. H. (1988). Hindered settling of semidilute monodisperse and polydisperse suspensions. *A.I.Ch.E. Journal*, *34*, 123–129.

Davis, R. H., & Gecol, H. (1994). Hindered settling function with no empirical parameters for polydisperse suspensions. *A.I.Ch.E. Journal*, *40*(3), 570–575.

Davis, R. H., & Hassen, M. A. (1988). Spreading of the interface at the top of a slightly polydisperse sedimenting suspension. *Journal of Fluid Mechanics*, *196*, 107–134.

Galvin, K. P., Pratten, S., & Nguyen Tran Lam, G. (1999). A generalized empirical description for particle slip velocities in liquid fluidized beds. *Chemical Engineering Science*, *54*, 1045–1052.

Greenspan, H. P., & Ungarish, M. (1982). On hindered settling of particles of different sizes. *International Journal of Multiphase Flow*, *8*, 587–604.

He, L. Z., Gan, Y. R., & Sun, Y. (1997). Adsorption-desorption of BSA to highly substituted dye-ligand adsorbent: Quantitative study of the effect of ionic strength. *Bioprocess Engineering*, *17*(5), 301–305.

Huppert, H. E., Kerr, R. C., Lister, J. R., & Turner, J. S. (1991). Convection and particle entrainment driven by differential sedimentation. *Journal of Fluid Mechanics*, *226*, 349.

Khan, A. R., & Richardson, J. F. (1989). Fluid–particle interactions and flow characteristics of fluidized beds and settling suspensions of spherical particles. *Chemical Engineering Communications*, *78*, 111–130.

Kumar, S., Pirog, T. W., & Ramkrishna, D. (2000). A new method for estimating hindered creaming/settling velocity of particles in Polydisperse Systems. *Chemical Engineering Science*, *55*, 1893–1904.

Kurganov, A., & Tadmor, E. (2000). New high-resolution central schemes for nonlinear conservation laws and convection-diffusion equations. *Journal of Computational Physics*, *160*, 241–282.

Kynch, G. J. (1952). A theory of sedimentation. *Transactions of the Faraday Society*, *48*, 166–176.

Law, H.-S., Masliyah, J. H., MacTaggart, R. S., & Nandakumar, K. (1987). Gravity separation of bidisperse suspensions: Light and heavy particle species. *Chemical Engineering Science*, *42*(7), 1527–1538.

Masliyah, J. H. (1979). Hindered settling in a multi-species particle system. *Chemical Engineering Science*, *34*, 1166–1168.

Nessyahu, H., & Tadmor, E. (1990). Non-oscillatory central differencing for hyperbolic conservation laws. *Journal of Computational Physics*, *87*, 408–463.

Owen, R. O., & Chase, H. A. (1997). Direct purification of lysozyme using continuous counter-current expanded bed adsorption. *Journal of Chromatography A*, *757*, 41–49.

Patwardhan, V. S., & Tien, C. (1985). Sedimentation and liquid fluidization of solid particles of different sizes and densities. *Chemical Engineering Science*, *40*(7), 1051–1060.

Shih, Y. T., Gidaspow, D., & Wasan, D. T. (1986). Sedimentation of fine particles in nonaqueous media Part I—Experimental Part II—Modeling. *Colloids Surfaces*, *21*, 393–429.

Shih, Y. T., Gidaspow, D., & Wasan, D. T. (1987). Hydrodynamics of sedimentation of multisized particles. *Powder Technology*, *50*, 201–215.

Smith, T. N. (1966). The sedimentation of particles having a dispersion of sizes. *Transactions of the Institution of Chemical Engineers*, *44*, 153–157.

Stamatakis, K., & Tien, C. (1988). Dynamics of batch sedimentation of polydisperse suspensions. *Powder Technology*, *56*, 105–117.

Stolojanu, V., & Prakash, A. (2001). Characterization of slurry systems by ultrasonic techniques. *Chemical Engineering Journal*, *84*, 215–222.

Wallis, G. B. (1969). *One-dimensional two-phase flow*. New York: McGraw-Hill.

Weast, R. C. (1988). *CRC Handbook of Chemistry and Physics* (69th ed.). Boca Raton, FL: CRC Press Inc.

Willoughby, N. A., Hjorth, R., & Titchener-Hooker, N. J. (2000). Experimental measurement of particle size distribution and voidage in an expanded bed adsorption system. *Biotechnology and Bioengineering*, *69*, 648–653.

Xue, B., & Sun, Y. (2001). Protein adsorption equilibria and kinetics to a poly(vinyl alcohol)-based magnetic affinity support. *Journal of Chromatography A*, *921*(2), 109–119.